IEEE Access
Multidisciplinary ⋮ Rapid Review ⋮ Open Access Journal

Received 12 June 2023, accepted 1 July 2023, date of publication 20 July 2023, date of current version 28 July 2023.

Digital Object Identifier 10.1109/ACCESS.2023.3297219

RESEARCH ARTICLE

Design Optimization of Battery-Electric Marine Vessels via Geometric Programming

ANTTI RITARI, PANAGIOTIS MOURATIDIS, AND KARI TAMMI, (Member, IEEE)
Department of Mechanical Engineering, Aalto University, 02150 Espoo, Finland

Corresponding author: Antti Ritari (antti.ritari@aalto.fi)

This work was supported by Clean Propulsion Technologies Research Project through Business Finland under Grant 38485/31/2020.

ABSTRACT This paper proposes formulating conceptual-stage vessel design optimization problems as geometric programs, which can be transformed into convex optimization problems. Convex optimization offers significant advantages in efficiency, reliability and automation potential over the general nonlinear optimization approach typically used in naval architecture. Focusing on battery-electric vessels, geometric program compatible models are derived for lithium-ion cells, power converters, propulsion motors and propellers. Preliminary hull form development, stability calculation and structural design are also presented in the context of geometric programming. The modeling approach is applied to study optimal battery sizing for a coastal bulk carrier sailing in varying operational conditions. Using open-source software tools, the battery sizing problem is solved in less than a second on a standard desktop computer. Local sensitivity information encoded by optimal dual variables reveals that increasing the cell discharge upper bound by 1% decreases the optimal total number of cells by more than 1%. On the other hand, the sensitivities of cell volume and maximum discharging current parameters are zero, indicating that the constraints involving these parameters do not govern the solution.

INDEX TERMS Electric propulsion, battery energy storage, design, optimization, convex optimization, geometric programming.

I. INTRODUCTION

A. ZERO EMISSION PATHWAYS

The maritime shipping industry is accelerating the search for economically and technically viable zero-emission alternatives to conventional fossil fuels. Electricity generated by renewable sources provides a zero-emission pathway through either substitution of conventional fuels by electrofuels (e-fuels) or by direct electrification. The latter concept refers to storing electrical energy onboard the vessel using battery energy storage in combination with electric propulsion driveline. The direct electrification pathway is typically at least four times more efficient than the e-fuel pathway [1].

Rapid cost decline and energy density improvement of lithium-ion batteries are driving the direct electrifcation pathway. In another recent work [2], the authors evaluate the feasiblity of battery electrification for container carriers and find it favorable for vessels over 8000 TEU with voyages less than 1000 kilometers. The authors assume figures 470 Wh/l for volumetric energy density and 94 €/kWh for the cost of lithium-ion batteries, reflecting a realistic near-future scenario.

B. DESIGN OF BATTERY-ELECTRIC VESSELS

The key technical challenge for battery-electric vessels arises from the extra volume and weight of the battery system, propulsion motor, and power electronics relative to the volume of internal combustion engines and fuel tanks of conventional vessels. Current commercially available lithium-ion battery cells exhibit at least two orders of magnitude lower volumetric energy density than liquid hydrocarbon fuels [3]. The additional weight and volume impact draught, resistance, hydrodynamics, aerodynamics, stability, and energy consumption of vessels.

The associate editor coordinating the review of this manuscript and approving it for publication was Qinfen Lu.

The conventional design process, which relies on statistical data from similarly built vessels [4], is inadequate for the design of novel battery-electric vessel concepts. In the conventional approach, the design parameters (length, displacement, block coefficient, length-to-breadth-ratio, etc.) are calculated using empirical formulae, tabular values and regression equations [5]. The advantages of this approach are simplicity and speed. However, vessels in the database could be poor designs which in turn impact all the vessels that follow [4]. Another disadvantage is the poor reliability of data. Useful data is likely missing for design tasks that employ novel battery-electric architecture.

C. LOCAL SEARCH METHODS

The design should be derived from first principles when the design is new, uncommon and data is lacking from similar existing vessels [4]. First principles analysis requires that physical relationships and performance bounds be described analytically as equations and inequalities. Given an initial guess (starting point), a classical local search method can be employed to seek a locally optimal design. Steepest descent and sequential quadratic programming are classical general-purpose local search methods that iterate an initial solution towards a locally optimal solution by incorporating first and second derivatives. However, the optimal design can possibly be located far away from the one found within the search space. Another shortcoming is the failure to determine feasibility in a reliable manner. Local methods can fail to find a feasible design even though one exists.

Using a local optimization method involves experimenting with the choice of algorithm and initial guess of optimization variables as well as adjusting algorithm parameters. The typical approach is to start the search from many different initial designs and take the best final design found. This approach increases the likelihood of finding the globally optimal design but does not guarantee it, while the computational effort increases with the number of initial guesses.

D. GLOBAL SEARCH METHODS

Global search methods aim to avoid becoming trapped in a locally optimal design by employing stochasticity in the search process. Genetic algorithms are the most commonly used global methods in vessel design [6], [7], [8]. Genetic algorithms are based on a population of individual solutions that evolves toward an optimal solution over generations, mimicking the process of biological evolution. Other global methods involve particle swarms and simulated annealing.

Although these methods can, in principle, compute the global solution, in practice, there is no guarantee. Achieving complete confidence that the global design has been found within a given tolerance comes at a computational cost that is prohibitive for practical design problems. Even without a guarantee of global optimality, solution times for practical problems in the industry typically range from hours to days [9].

E. CONVEX OPTIMIZATION

The aim of this study is to propose a convex programming framework for the conceptual-stage design optimization of battery-electric vessels. The vessel design problem is formulated as a special type of optimization problem, called a geometric program (GP). The key feature of GPs is that they can be reformulated as convex optimization problems. Open-source interior point algorithms can solve convex optimization problems with tens of thousands of variables and constraints reliably in only a few seconds on a standard desktop computer [10].

Vessel design problems cast as GPs can be globally solved, which has important practical implications. Infeasible problems are unambiguously identified. The solution algorithm either produces a feasible point or a proof that the specification is infeasible. The choice of the initial point (representing the initial design) has no effect on the final design that is obtained by the optimization procedure. Thus, the quality of the final design does not depend on the naval architect's skill in selecting a good initial point. Since the optimization procedure is guaranteed to find the global optimum, given that the design problem is feasible, the vessel design obtained represents the absolute limit of performance for given design constraints.

The availability of extremely efficient solution methods for convex problems also has a number of important practical implications. The efficiency can be exploited to obtain designs that are guaranteed to meet a set of specifications over a variety of parameter values. The variety arises from a large number of operational scenarios derived from historical weather conditions of planned routes or operational data of similar vessels.

The speed and reliability of the GP modeling framework are emphasized in extensive exploration of the design space. The endurance and speed requirements and component performance parameters can be swept over a range of values to study when the design becomes infeasible or constraints become activated. Since solving a single design problem takes only a few seconds, even large sweeps over multiple parameters can be completed quickly. Thus, system level optimization can be applied at the very beginning of the design process which leads to fewer changes in the latter design stages and fewer associated costs.

F. CONTRIBUTION

The main contribution of this paper is to demonstrate that the conceptual-stage battery-electric vessel design problem can be formulated as a GP. Once formulated as a GP, the problem can be transformed into a convex optimization problem and solved efficiently and reliably using off-the-shelf solvers. The convex optimization problem formulation brings a number of advantages over current methods widely used in the maritime sector.

GP modeling has found success in many areas of engineering design that are related to subproblems in the

vessel design workflow. These subproblems include the design of three-dimensional layouts [11], transformers [12], and aerodynamic structures subjected to drag [13]. However, to the knowledge of the authors, the GP framework has not previously been applied to marine vessel design optimization.

II. PROBLEM DESCRIPTION

The vessel design process progresses in stages, beginning with the definition of requirements, then advancing to concept design, contract design and finally to detail design and manufacturing. At each stage, decisions are locked, imposing constraints for later stages and increasing the cost of making changes [9]. Key decisions regarding design trade-offs must be made early in the process when design knowledge is most limited.

The conceptual design stage aims at understanding the key design trade-offs. The design problem typically consists of many objectives that are in conflict with each other or may be poorly defined in the beginning [9]. The objective can be a single quantity, such as the total cost of ownership, or a weighted combination of several quantities of interest. In the most simple form, a function to be minimized is formulated as the total number of cells in the battery pack and the performance requirements are encoded as a set of constraints.

Requirements are system-level performance bounds imposed by the naval architect. These are simple expressions, e.g., payload, minimum range between bunkering or charging (endurance) and design speed with sea margin. Underlying physics is encoded as equations. Engineering limits impose practical limits on the design quantities: stresses, deflections, and margins of safety.

The major subsystems have recursive design relationships. For example, towing resistance depends on the wetted surface area of the hull, which depends on the weight of the vessel. The size of the battery pack depends on the towing resistance, which depends on the weight of the battery pack. Similarly, resistance, longitudinal strength and transverse stability are strongly coupled.

In summary, the main tasks of the conceptual design stage are:

1) Selection of main dimensions;
2) Hull form development;
3) Resistance and propulsion estimations;
4) Selection of energy carriers, energy storage devices, and energy converters;
5) Analysis of energy saving devices;
6) Development of internal layout;
7) Preliminary structural design;
8) Weight estimation;
9) Intact and damage stability calculations;
10) Assessment of economic performance.

Explosion and fire hazard risks are emphasized in high-energy battery-electric vessels. Classification societies impose rules regarding the safety aspects of marine battery systems. In case of a fire in a cell, propagation must be prevented by either insulating each cell, or alternatively limiting the propagation to a group of cells with total capacity less than 11 kWh [14]. Fire risk and potential toxic gas development is managed by locating all battery system components to a dedicated battery space in the vessel. The battery space boundaries must be vessel structures and the space requires continuously running mechanical ventilation.

III. GEOMETRIC PROGRAMMING

In the context of geometric programming, we refer to a *posynomial* as a function of real positive variables $x \in \mathbb{R}^n_{++}$ of the form

$$f(x) = \sum_{k=1}^{K} c_k \prod_{i=1}^{n} x_i^{a_{i,k}}, \tag{1}$$

where $c_k > 0$ are constant coefficients and $a_{i,k} \in \mathbb{R}$ are (possibly negative or fractional) constant exponents. If $K = 1, f$ is called a *monomial*.

A GP is a problem of the form:

$$\begin{aligned} \min_x \quad & f_0(x) \\ \text{s.t.} \quad & f_i(x) \le 1, \quad i = 1, \ldots, m \\ & g_i(x) = 1, \quad i = 1, \ldots, p \end{aligned} \tag{2}$$

where f_i are posynomials and g_i are monomials. Since a GP is a nonlinear and nonconvex optimization problem, it is not readily amenable to efficient and reliable solution.

A. CONVEX FORM OF A GP

The special structure of a GP allows it to be transformed to a nonlinear, but *convex* optimization problem, i.e., a problem with convex objective and inequality constraint functions, and linear equality constraint. The transformation is based on a logarithmic change of variables, and a logarithmic transformation of the objective and constraint functions. The details of the transformation are given in [10].

As a simple example, we consider the log-transformation of the propeller torque relation (introduced in Sec. IV-F)

$$K_Q = \frac{M_p}{\rho_{\text{sw}} D_p^5 n_p^2}$$

with variables K_Q, M_p, D_p and n_p. The above equation defines a nonconvex set. With new variables $\bar{K}_Q = \log K_Q, \bar{M}_p = \log M_p, \bar{D}_p = \log D_p$ and $\bar{n}_p = \log n_p$ the equation takes the form

$$\rho_{\text{sw}} e^{\bar{K}_Q} e^{5\bar{D}_p} e^{2\bar{n}_p} e^{-\bar{M}_p} = 1.$$

Applying the function log-transformation yields

$$\begin{aligned} & \log\left(\rho_{\text{sw}} e^{\bar{K}_Q} e^{5\bar{D}_p} e^{2\bar{n}_p} e^{-\bar{M}_p}\right) = \log 1 \\ \Rightarrow\ & \log \rho_{\text{sw}} + \bar{K}_Q + 5\bar{D}_p + 2\bar{n}_p - \bar{M}_p = 0, \end{aligned}$$

where the left-hand side is a linear expression and the equation defines a convex set.

B. FORMULATING AND SOLVING CONVEX PROBLEMS

Domain-specific languages (DSLs) for convex optimization are programming languages for specifying convex optimization problems. DSLs support syntax that follows the mathematical description of the problem. In the GP case, user specifies the posynomial and monomial functions for the problem instance. DSLs parse the input, log-transform the variables and functions, and translate the problem to a standard form that solvers accept. Examples of DSLs include CVX [15] in MATLAB and CVXPY [16] in Python.

Standard open-source solvers such as ECOS [17], OSQP [18] and SCS [19] can be used. When applied to solve convex programs, the solvers [10]:

1) Provide a certificate on infeasibility if no point exists that simultaneously satisfies all the constraints;
2) Guarantee convergence to a global optimum given that the problem is feasible;
3) Achieve speed that compares to linear programming solvers, which means that in practice, problems with many thousands of variables and constraints can be solved in a few seconds on a standard desktop computer;
4) Determine globally optimal values for dual variables, which express how tightly constrained the problem is with respect to each constraint.

Convex optimization solvers do not require the user to make initial guesses, tune optimizer parameters or evaluate the quality of the solution. This is in stark contrast to methods for general nonlinear optimization.

C. MULTICRITERION GP

A GP with q different scalar objectives, each of which is to be minimized, is expressed as a vector optimization problem:

$$\begin{aligned} \min_x \ (\text{w.r.t. } \mathbb{R}_+^q) \quad & f_0(x) \\ \text{s.t.} \quad & f_i(x) \leq 1, \quad i = 1, \ldots, m \\ & g_i(x) = 1, \quad i = 1, \ldots, p \end{aligned} \tag{3}$$

where f_i are posynomials, g_i are monomials and f_0 is a vector with elements $(F_1, \ldots, F_q)$ of posynomial objectives.

An optimal point x^* for the multicriterion problem is a point that is simultaneously optimal for each objective $F_1, \ldots, F_q$ [10]. However, typical multicriterion vessel design problem has competing (or conflicting) criteria and no optimal point exists. Instead, the aim is to identify Pareto optimal points from the set of achievable values. Solving the multicriterion problem entails obtaining a set of Pareto optimal values, which can be interpreted as a trade-off surface between the competing objectives.

The scalarized multicriterion GP is formulated by forming a scalar objective function that is a sum of objectives $F_1, \ldots, F_q$ multiplied by weights $\lambda_1, \ldots, \lambda_q$:

$$\lambda^T f_0(x) = \sum_{i=1}^{q} \lambda_i F_i(x). \tag{4}$$

Regardless of the values that the weights $\lambda_1, \ldots, \lambda_q$ receive, i.e., prioritization of each objective, if x^* is an optimal point for the scalarized problem, then x^* is an efficient point (Pareto optimal) for the original multicriterion vector problem [10]. This insight enables a solution strategy for the multicriterion problem. By solving a sequence of regular scalar optimization problems with varying weight vector, different Pareto optimal solutions are obtained. Since the log transformation of a GP yields a convex problem, and for convex problems scalarization yields all Pareto optimal points, all Pareto optimal points are obtained for a GP.

D. SENSITIVITY ANALYSIS

A perturbed GP is defined as:

$$\begin{aligned} \min_x \quad & f_0(x) \\ \text{s.t.} \quad & f_i(x) \leq e^{u_i}, \quad i = 1, \ldots, m \\ & g_i(x) = e^{v_i}, \quad i = 1, \ldots, p \end{aligned} \tag{5}$$

where u_i and v_i are relative perturbations of the constraints [10]. If u_i and v_i are zeros, the perturbed problem equals the original problem. If $u_i < 0$, then the corresponding constraint is tightened compared to the original. If $u_i > 0$, the constraint is loosened. Let $f_0^*(u, v)$ denote the optimal objective value as a function of the parameters u_i and v_i such that the original objective value is $f_0^*(0, 0)$. Variation of f_0^* as a function of small changes in u and v, is called sensitivity analysis. The relative change in objective is expressed as:

$$S_i = \frac{\partial \log f_0^*}{\partial u_i}, \quad T_i = \frac{\partial \log f_0^*}{\partial v_i} \tag{6}$$

evaluated at $(0, 0)$. The key insight is that a standard solver using an interior-point method returns the sensitivities S_i and T_i by default from the solution of the dual problem [10]. The sensitivity values are useful in practical engineering design, because they tell how tightly constrained the problem is with respect to each constraint.

Perturbations in the model's parameters corresponds to tightening or loosening of one or more constraints. Using chain rule and optimal dual variable values, we can compute the relative change of the objective to any combination of simultaneous parameter perturbations [20].

E. FITTING GP COMPATIBLE SURROGATE FUNCTIONS TO DATA

If an equation in the vessel model cannot be manipulated algebraically into forms required by GP, a GP compatible model may be fitted to approximate the original relationship in a restricted range. This fitting procedure can also be applied to make models encoded by simulation data available in an analytical form, e.g., by using data from CFD and hydrostatics simulations.

The approximation procedure begins with sampling l data points from the original GP incompatible model or computational routine:

$$(x_i, y_i) \in \mathbb{R}^n_{++} \times \mathbb{R}_{++},\ i = 1, \ldots, l.$$

The log-transformation $(z_i, w_i) = (\log x_i, \log y_i)$ generates the data

$$(z_i, w_i) \in \mathbb{R}^n \times \mathbb{R},\ i = 1, \ldots, l.$$

A convex function is fitted to the transformed data using standard nonlinear regression method. Convex functions belonging to the class of softmax-affine (SMA) have been observed to work well in practice with only a small number of terms [21]. This class of functions has the log-sum-exp form

$$f_{\mathrm{SMA}}(z) = \frac{1}{\alpha} \log \sum_{k=1}^{K} \exp(\alpha(b_k + a_k^T z)), \tag{7}$$

where the fitted model parameters are $\alpha > 0$, $a_k \in \mathbb{R}^n$ and $b_k \in \mathbb{R}$. The number of user specified exp terms is K.

The SMA function corresponds to the posynomial constraint

$$\sum_{k=1}^{K} \exp(\alpha b_k) \prod_{i=1}^{n} x_i^{\alpha a_{ik}} \leq y^{\alpha}. \tag{8}$$

IV. GP COMPATIBLE VESSEL SUBSYSTEM MODELS

This section introduces GP compatible models for technical aspects of the battery-electric vessel design problem. A model refers to a relation that is expressed as either an inequality $f(x) \leq 1$ or an equation $g(x) = 1$ where f is a posynomial and g is a monomial. The symbols used in Sec. III will be redefined in this section and used consistently in the following sections.

A. DIMENSIONS AND FORM COEFFICIENTS

We first define the quantities that are relevant in preliminary hull resistance and displacement calculations. The length overall L_{OA} extends from the hull's foremost point to its aftmost point. In resistance calculations the length of the water plane area, called waterline length L_{WL}, is more relevant. If the bow design is straight-edged and vertical, the difference between L_{WL} and L_{OA} is negligible.

Draught T describes the vertical distance between the hull's deepest point and the waterline plane. Under normal conditions the foremost and the aftmost draughts are the same. Moulded depth D describes the vertical distance from the keel to the freeboard deck. Another key quantity is breadth at the waterline B_{WL}.

Displacement is the mass of the water displaced by a floating vessel. The volume of displacement is denoted ∇ and it depends on the mass density of the water [4], [22].

Various form coefficients are used to express the shape of the hull. The most important of these coefficients is the block coefficient C_B that is defined as the ratio between the displacement volume ∇ and the volume of a box with dimensions $L_{\mathrm{WL}} B_{\mathrm{WL}} T$:

$$C_B = \frac{\nabla}{L_{\mathrm{WL}} B_{\mathrm{WL}} T}. \tag{9}$$

Displacement volume cannot exceed the volume of the box, which imposes $C_B \leq 1$. The expression for C_B is a monomial and thus compatible with the GP framework.

Other commonly used hull form coefficients are water plane area C_{WL}, midship section coefficient C_M, prismatic coefficient C_P and fineness ratio C_{LD}. The cofficients are expressed, respectively, as monomials

$$C_{\mathrm{WL}} = \frac{A_{\mathrm{WL}}}{L_{\mathrm{WL}} B_{\mathrm{WL}}}, \tag{10}$$

$$C_M = \frac{A_M}{B_{\mathrm{WL}} T}, \tag{11}$$

$$C_P = \frac{\nabla}{L_{\mathrm{WL}} A_M}, \tag{12}$$

$$C_{\mathrm{LD}} = \frac{L_{\mathrm{WL}}}{\sqrt[3]{\nabla}}, \tag{13}$$

where A_{WL} is waterline area.

B. HULL GEOMETRY AND DISPLACEMENT

Hydrostatic calculations and design variations with parametric models are standard features in naval architecture software tools. These tools support hull form definition as parametric polynomial curves and respective surfaces [8]. Datasets generated by hydrostatics software can be included in the GP framework by fitting a posynomial models to the data as describe in Sec. III-E. However, in this and the following sections, we consider a hull model in analytical form and derive closed form expressions for the relevant quantities.

We consider a set H of hull sections with varying geometry. A Cartesian coordinate system denoted XYZ is used to give the surface geometry of a hull section. The origin of the coordinate system is located at the foremost point at the keel centerline of the section. The X-axis is the lateral horizontal axis pointing to port side, Y-axis is the longitudinal horizontal axis pointing to the direction of stern and the Z-axis points upwards. The surface geometry of a section $j \in H$ is the set of points with coordinates (x, y, z) that satisfy $z = f_j(x, y)$, where $f_j : \mathbb{R}^2 \to \mathbb{R}$ is a smooth function that is strictly increasing in x for all $y > 0$.

Let L_j denote the length of a section in longitudinal Y-axis. For the breadth on freeboard deck B and breadth on waterline B_{WL}, the following hold:

$$\max_{y \in [0, L_j]} f(B_{\mathrm{WL}}, y) = T, \tag{14}$$

$$\max_{y \in [0, L_j]} f(B, y) = D \tag{15}$$

for all $j \in H$.

An elementary hull form can be assembled from only three sections, as illustrated in Figs. 1 and 2. The geometry

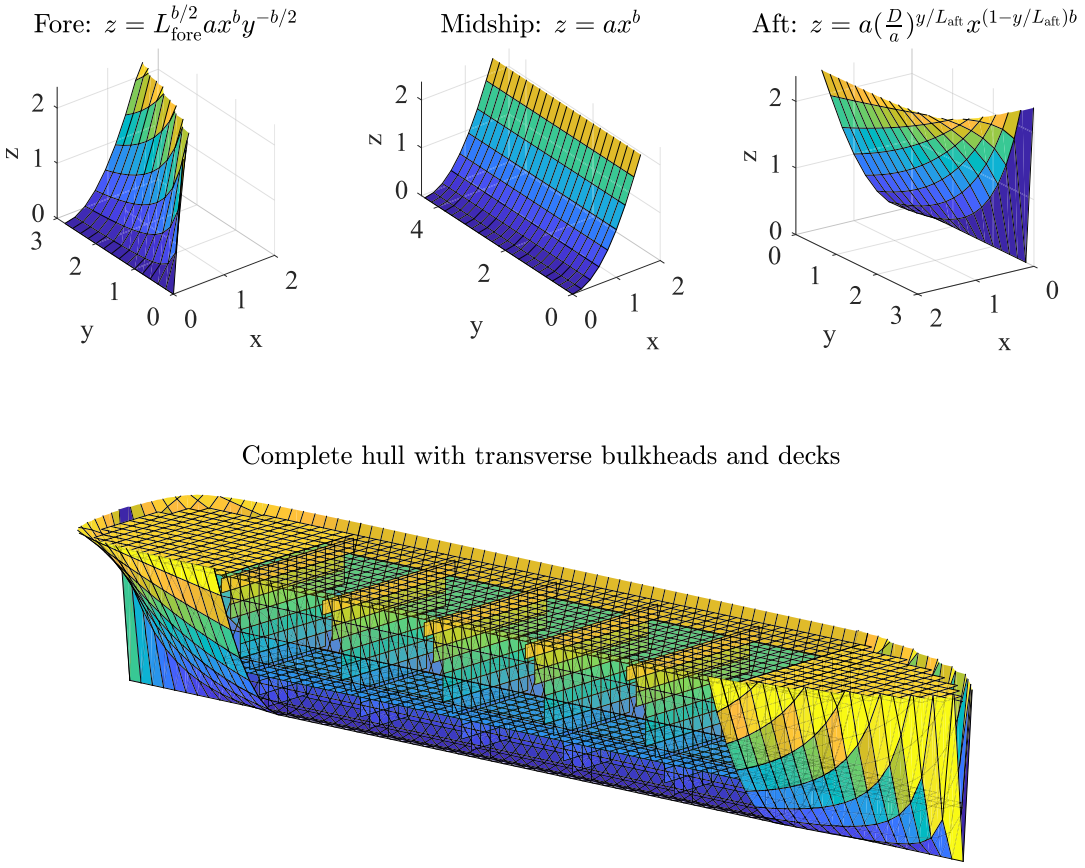

FIGURE 1. Composition of an analytical hull model.

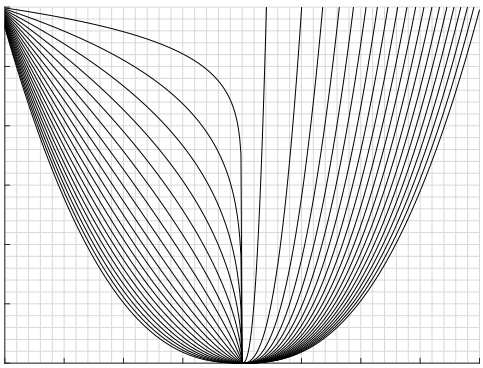

FIGURE 2. Body plan of a vessel with hull fullness $b = 2.5$.

functions f_j, $j \in \{\text{aft}, \text{mid}, \text{fore}\}$, are parameterized by L_j and form coefficients a and b. The contribution of each hull section to steel weight, displacement and wetted surface area is required in the preliminary design calculations. Next, we'll focus on the midship and fore sections and illustrate the derivation of a section's contribution to the displacement volume at draught T by means of definite integrals.

The geometry of the midship section is uniform in the longitudinal direction. Thus, we can write the volume under the surface of the section, denoted $V_{\text{mid,under}}$, as a single integral:

$$\begin{aligned} V_{\text{mid,under}} &= L_{\text{mid}} \int_0^{\left(\frac{T}{a}\right)^{1/b}} ax^b \, dx \\ &= L_{\text{mid}} a \left[\frac{x^{b+1}}{b+1} \right]_0^{\left(\frac{T}{a}\right)^{1/b}} \\ &= \frac{L_{\text{mid}} T \left(\frac{T}{a}\right)^{1/b}}{b+1}. \end{aligned} \tag{16}$$

The volume of a cuboid that encloses the midship section at the waterline is

$$V_{\text{mid,block}} = \frac{L_{\text{mid}} T B_{\text{WL}}}{2} = L_{\text{mid}} T \left(\frac{T}{a}\right)^{1/b}. \tag{17}$$

Given that b is a fixed parameter, the expressions (16) and (17) are monomials. The volume of displaced water relates to the volumes defined above according to

$$\frac{1}{2}\nabla_{\text{mid}} = V_{\text{mid,block}} - V_{\text{mid,under}}, \tag{18}$$

which can be relaxed to a valid posynomial inequality

$$\nabla_{\text{mid}} + 2V_{\text{mid,under}} \leq 2V_{\text{mid,block}}. \tag{19}$$

The fore section exhibits curvature in two directions, and the volumes enclosed by the section are given by double integrals. We consider the following three volumes:

1) $V_{\text{fore,block}}$, volume of a cuboid that encloses the hull section at the waterline:

$$V_{\text{fore,block}} = \frac{L_{\text{fore}} T B_{\text{WL}}}{2}; \tag{20}$$

2) $V_{\text{fore,under}}$, volume under the surface of the section:

$$\begin{aligned} V_{\text{fore,under}} &= L_{\text{fore}}^{b/2} a \int_0^{L_{\text{fore}}} \int_0^{\left(\frac{T y^{b/2}}{L_{\text{fore}}^{b/2} a}\right)^{\frac{1}{b}}} \frac{x^b}{y^{b/2}}\, dx\, dy \\ &= L_{\text{fore}}^{b/2} a \int_0^{L_{\text{fore}}} \frac{1}{y^{b/2}} \left[\frac{x^{b+1}}{b+1}\right]_0^{\left(\frac{T y^{b/2}}{L_{\text{fore}}^{b/2} a}\right)^{\frac{1}{b}}} dy \\ &= \frac{L_{\text{fore}}^{b/2} a}{b+1} \left(\frac{T}{L_{\text{fore}}^{b/2} a}\right)^{1+1/b} \int_0^{L_{\text{fore}}} y^{b/2+1}\, dy \\ &= \frac{2 L_{\text{fore}} T \left(\frac{1}{T}\right)^{-1/b}}{3(b+1)}; \end{aligned} \tag{21}$$

3) $V_{\text{fore,res}}$, residual volume, i.e., the volume between the cuboid and a vertical surface following the edge of the section:

$$\begin{aligned} V_{\text{fore,res}} &= T \frac{L_{\text{fore}}^{b/2} a}{T} \int_0^{\left(\frac{T}{a}\right)^{1/b}} x^b\, dx \\ &= L_{\text{fore}}^{b/2} a \left[\frac{x^{b+1}}{b+1}\right]_0^{\left(\frac{T}{a}\right)^{1/b}} \\ &= \frac{L_{\text{fore}} T}{3} \left(\frac{1}{T}\right)^{-1/b}. \end{aligned} \tag{22}$$

The volume of displaced water at draught T relates to the volumes above according to

$$\frac{1}{2}\nabla_{\text{fore}} = V_{\text{fore,block}} - (V_{\text{fore,res}} + V_{\text{fore,under}}), \tag{23}$$

which attains a GP compatible form when relaxed to an inequality

$$\nabla_{\text{fore}} + 2V_{\text{fore,res}} + 2V_{\text{fore,under}} \leq 2V_{\text{fore,block}}. \tag{24}$$

C. HULL RESISTANCE

A body moving through a liquid will encounter dynamic pressure according to Bernoulli's law [22]:

$$p_{\text{dyn}} = \frac{\rho_{\text{sw}}}{2} v^2, \tag{25}$$

where ρ_{sw} is density of seawater and v is the speed of the vessel. The dynamic pressure acts on the submerged surface of the vessel, the so-called wetted area A_s and results in a reference force K [22]:

$$K = \frac{\rho_{\text{sw}}}{2} A_s v^2. \tag{26}$$

The wetted area is given by integrating over the surfaces specified by the analytical hull section models. However, the surface integrals do not yield closed from expressions in general. We can instead approximate the total area by breaking up the interval $[0, T]$ into a number of subintervals, computing an approximation for each subinterval by closed form surface integral, and then adding up. Approximation of the arc length r_T for the midship section from keel to waterline (0 to T) by N_{arc} segments is

$$\begin{aligned} r_{T,\text{mid}} &\approx \sum_{i=0}^{N_{\text{arc}}-1} \sqrt{\left(\frac{1}{N_{\text{arc}}}\left(\frac{T}{a}\right)^{1/b}\right)^2 + \left(\frac{Tb}{N_{\text{arc}}^b}\left(\frac{1}{2}+i\right)^{b-1}\right)^2}. \end{aligned} \tag{27}$$

Although the right-hand side of (27) is not a posynomial, in this case we can reformulate it as a posynomial by introducing new variables and inequalities. The new variables $t_0, \ldots, t_{N_{\text{arc}}-1}$ relate to the terms in (27) via posynomial inequalities

$$\left(\frac{1}{N_{\text{arc}}}\left(\frac{T}{a}\right)^{1/b}\right)^2 + \left(\frac{Tb}{N_{\text{arc}}^b}\left(\frac{1}{2}+i\right)^{b-1}\right)^2 \leq t_i \tag{28}$$

for all $i = 0, \ldots, N_{\text{arc}} - 1$. We can now write (27) as a valid posynomial inequality

$$r_{T,\text{mid}} \geq \sum_{i=0}^{N_{\text{arc}}-1} t_i^{0.5}. \tag{29}$$

Having obtained an estimate of the arc length from keel to waterline, the midship wetted area is written simply as $A_{s,\text{mid}} = r_{T,\text{mid}} L_{\text{mid}}$. The wetted areas of the aft and fore elements can be estimated based on $A_{s,\text{mid}}$ or by a more elaborate integration scheme.

The reference force K and the dimensionless total calm water resistance coefficient C_t are used to calculate the hull's total calm water resistance R_T:

$$R_T = C_t K = \frac{\rho_{\text{sw}}}{2} C_t A_s v^2. \tag{30}$$

The total calm water resistance and the total calm water resistance coefficient can be split into several components. The most important coefficient components are the friction coefficient C_F and the residual resistance coefficient C_R:

$$C_t = C_R + C_F. \tag{31}$$

The frictional resistance constitutes 50-90% of the overall resistance [22]. This percentage depends on the vessel's speed and is higher for slow vessels. The frictional resistance is explained by two phenomena. First, it considers the friction caused by a plate with equivalent length and wetted surface area. Second, it takes into account the additional friction caused by the hull's curvature.

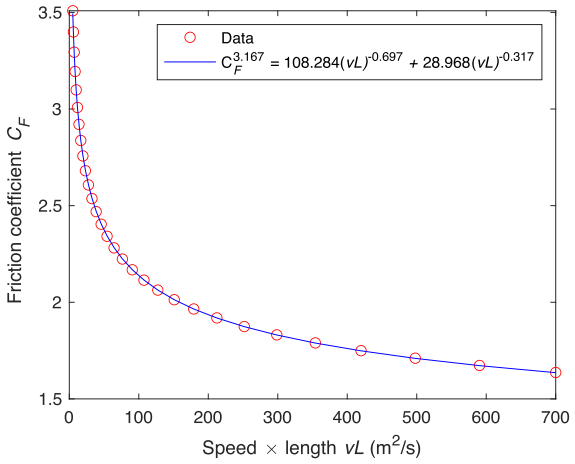

FIGURE 3. Posynomial fit of data for friction coefficient C_F as a function of vL. The RMS error of the softmax-affine function (K=2) fit is 9.18e-4.

According to the guidelines [23] the friction coefficient is approximated as

$$C_F = \frac{0.075}{(\log_{10}(\mathrm{Re}) - 2)^2}, \quad \mathrm{Re} = \frac{vL}{\nu}, \tag{32}$$

where Re is Reynold's number and ν is kinematic viscosity of the fluid. To avoid numerical problems due to very small value of ν, the formulation is rearranged:

$$C_F \times 10^3 = \frac{75}{(\log_{10}(vL) \underbrace{- \log_{10}(\nu)}_{>0} - 2)^2}, \tag{33}$$

where the right-hand side is not log-convex with respect to v and L for all $vL > 0$. However, the right-hand side is log-convex for vL range [1e2,1e3] that is relevant in vessel design problems. In this case a GP compatible posynomial can be fitted following the procedure introduced in Sec. III-E (Fig. 3). Similarly, the residual coefficient can be obtained in an analytical form by fitting a posynomial to data generated by CFD simulation.

The resistance model can be written in GP compatible form as the posynomial inequality:

$$R_T \geq \frac{\rho_{\mathrm{sw}}}{2}(C_F + C_R)A_s v^2. \tag{34}$$

D. LONGITUDINAL STRENGTH

Decks, bulkheads, side and bottom plating along with the longitudinal framing system form the closed load carrying mechanism of the hull called *hull girder*. Bending moment and shear forces are the primary load resultants acting on the hull girder. In the conceptual design phase, the structure is assumed to behave as a beam and the bending response follows Euler-Bernoulli beam theory [24].

According to the beam theory, normal stress at distance z from the beam neutral axis relates to the bending moment M as

$$\sigma_y = \frac{M}{I}z, \tag{35}$$

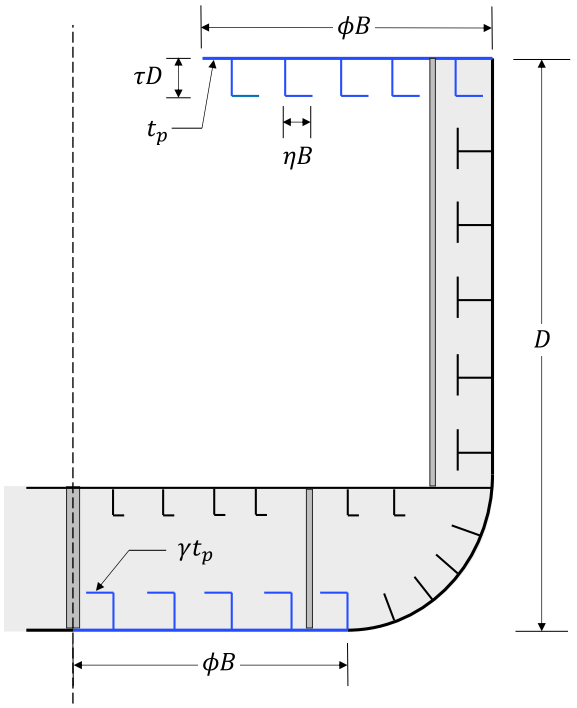

FIGURE 4. Schematic of the midship structural cross section geometry. Members contributing to the hull girder longitudinal strength are highlighted as blue.

where I is a geometrical property of the cross section, called second moment of area. The maximum values of the normal stresses are in the bottom shell and weather deck that are located furthest from the neutral axis. The second moment of area divided by the distance to bottom (or deck) from neutral axis gives the section modulus $Z = I/z$ in relation to the bottom (or deck), which is applied to calculate the ultimate strength of the hull girder.

We consider a symmetrical hull girder midship cross section (Fig. 4) of a longitudinally stiffened vessel, where the load carrying structural elements are the bottom shell, weather deck and the stiffeners. The L profile is composed of a horizontal part (flange) and vertical part (web). The widths of the plates and flanges are related to hull breadth B via the parameters ϕ and η, respectively. The height of the web related to depth D via parameter τ. The plate thickness t_p is a decision variable.

The second moment of area for the deck plate element is

$$\begin{aligned} I_{\mathrm{plate}} &= 2\frac{\phi B}{12}\left(D^3 - (D - 2t_p)^3\right) \\ &= \phi B\left(D^2 t_p - 2Dt_p^2 + \frac{2}{3}t_p^3\right). \end{aligned}$$

Since $D \gg t_p$ the term t_p^3 has negligible influence on I_{plate}. With this insight we use the approximation

$$I_{\mathrm{plate}} \approx \phi B\left(D^2 t_p - 2Dt_p^2\right). \tag{36}$$

The second moment of areas of the stiffener web and flange elements are

$$\begin{aligned} I_{\text{flange}} &= \frac{\eta B}{12}\left((\lambda D)^3 - (\lambda D - 2\gamma t_p)^3\right) \\ &\approx \frac{\eta B}{2}\left((\lambda D)^2 \gamma t_p - 2\lambda D(\gamma t_p)^2\right), \end{aligned} \tag{37}$$

$$\begin{aligned} I_{\text{web}} &= \frac{\gamma t_p}{12}\left(D^3 - (D - 2\tau D)^3\right) \\ &\approx \frac{\gamma B(\tau - 2\tau^2)}{2} D^2 t_p, \end{aligned} \tag{38}$$

where $\lambda = 1 - 2\tau$ and $D \approx B$ in the the last expression. With n_L denoting the number of stiffeners, the total midship second moment of area can now be written as a posynomial inequality

$$\begin{aligned} &I_{\text{mid}} + DBt_p^2(2\phi + n_L\eta\lambda\gamma^2) \\ &\quad \leq \frac{t_p BD^2}{2}(2\phi + n_L\eta\gamma\lambda^2 + n_L\gamma(\tau - 2\tau^2)). \end{aligned} \tag{39}$$

The distance from neutral axis to both deck and bottom is $D/2$. Thus, the section modulus for midship cross section geometry is

$$Z_{\text{deck}} = \frac{2I_{\text{mid}}}{D}. \tag{40}$$

Although the net buoyancy force and weight cancel out as a whole, they are unbalanced for each transverse section of the hull girder. This line load causes shear force and bending moment even in calm water. The vertical bending moment at each cross section can be obtained exactly by integrating the net force twice from the vessel's end.

In vessels with uniform midship section, e.g., bulk carriers, high block coefficient and even loading, the still water load is small compared to the contribution of waves. Thus, the ultimate strength is evaluated based on the negative wave bending moment, i.e., the sagging condition where the girder is bent downward [25]. Due to the irregular nature of waves, the vertical bending moment in the midship transverse section is calculated with an empirical formula combining calm water and negative wave moments:

$$M_{\text{wv+sw}} \approx 0.3365\, C_w B L^2, \tag{41}$$

where C_w is the wave coefficient.

Finally, the high level constraint of ultimate strength is

$$\sigma_{\text{perm}} \geq \frac{M_{\text{wv+sw}}}{Z_{\text{deck}}}. \tag{42}$$

E. INTACT TRANSVERSE STABILITY

Center of buoyancy is the centroid of the volume of water displaced by the submerged hull. When the vessel heels the center of buoyancy shifts while the center of gravity remains unchanged. The shifted center of buoyancy creates a moment arm between the vertical force vectors F_G and F_B (Fig. 5). If the moment acts to revert the vessel back to upright orientation, the vessel is initially stable.

Let A_{up} denote submerged area of midship half cross section with draught T in upright orientation as illustrated in Fig. 5 by a dashed horizontal line. Using the analytical expression $z = ax^b$ for the midship cross section geometry, the distance from keel to the center of buoyancy is given by first moment integral

$$\begin{aligned} z_B &= \frac{1}{A_{\text{up}}}\int_0^T z\left(\frac{z}{a}\right)^{1/b} dz \\ &= \frac{1}{A_{\text{up}}}\left(\frac{1}{a}\right)^{1/b}\int_0^T z^{(1/b+1)}\, dz \\ &= \frac{1}{A_{\text{up}}}\left(\frac{1}{a}\right)^{1/b}\frac{bT^{1/b+2}}{2b+1} \\ &= \frac{T(b+1)}{2b+1}, \end{aligned} \tag{43}$$

where

$$A_{\text{up}} = \int_0^T \left(\frac{z}{a}\right)^{1/b} dz = \left(\frac{1}{a}\right)^{1/b}\frac{bT^{1/b+1}}{b+1}. \tag{44}$$

Consider the right triangle that forms between the horizontal waterlines in upright orientation and heel by angle θ. Length of the adjacent side is $(T/a)^{1/b}$. The area and the location of the centroid from vertical centerline are

$$A_{\text{heel}} = \tan\theta\,\frac{1}{2}\left(\frac{T}{a}\right)^{2/b}, \tag{45}$$

$$x_{\text{heel}} = \frac{2}{3}\left(\frac{T}{a}\right)^{1/b}. \tag{46}$$

For small nonzero angle of heel, the shape of the submerged cross section can be composed from the shape in upright position and two triangle shapes. The location of the center of buoyancy is the location of the centroid of the composed form:

$$\begin{aligned} x_{B'} &= \frac{A_{\text{heel}}x_{\text{heel}} - A_{\text{heel}}(-x_{\text{heel}})}{2A_{\text{up}} + A_{\text{heel}} - A_{\text{heel}}} \\ &= \frac{2A_{\text{heel}}x_{\text{heel}}}{2A_{\text{up}}} = \frac{\tan\theta(b+1)(T/a)^{2/b}}{3Tb}. \end{aligned} \tag{47}$$

For small θ, the distance between p_M and p_B is

$$z_{\text{BM}} = \frac{x_{B'}}{\tan\theta} = \frac{(b+1)(T/a)^{2/b}}{3Tb}, \tag{48}$$

which is used to calculate metacentric height:

$$z_{\text{KM}} = \frac{(b+1)(T/a)^{2/b}}{3Tb} + \frac{T(b+1)}{2b+1}. \tag{49}$$

The moment from heel acts to revert the vessel back to upright orientation and the vessel is initially stable if the metacentric height is greater than the center of gravity: $z_{\text{KM}} > z_{\text{GK}}$. Imposing a safety margin via parameter $z_{\text{safe}} \geq 1$ yields a posynomial inequality for the stability condition:

$$\frac{(b+1)(T/a)^{2/b}}{3Tb} \geq (z_{\text{safe}} - 1)\frac{T(b+1)}{2b+1} + z_{\text{GK}}. \tag{50}$$

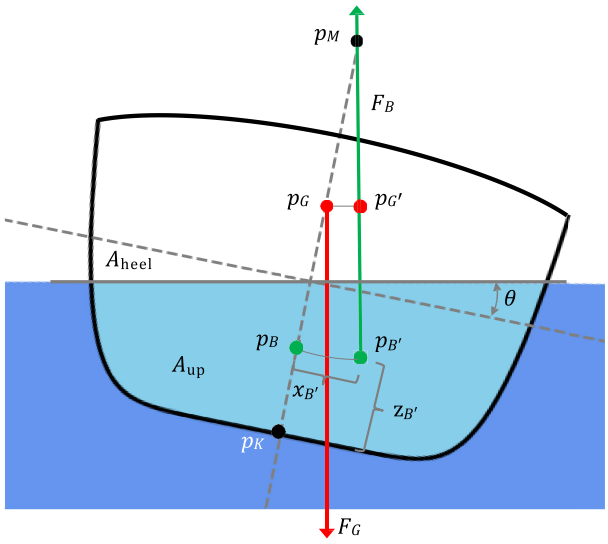

FIGURE 5. Shifting of center of buoyancy due to heel and the resulting moment arm.

F. PROPELLER TORQUE AND THRUST

Fixed pitch propellers are considered for propulsive thrust generation. The mathematical model needs to replicate thrust, torque and efficiency with sufficient accuracy, but it is not required to capture all hydrodynamic effects. The latter can be achieved with CFD software during the propeller design process, which is not in the scope of this work.

Independent from the specific design of a propeller, its performance can be described using its general open water characteristics [22]. These are based on the forces and momentums of the propeller when operating in open water without any disturbances and are usually expressed using the non-dimensional thrust coefficient

$$K_T = \frac{T_p}{\rho_{\text{sw}} D_p^4 n_p^2}, \tag{51}$$

torque coefficient

$$K_Q = \frac{M_p}{\rho_{\text{sw}} D_p^5 n_p^2}, \tag{52}$$

open water efficiency

$$\eta_o = \frac{P_{p,\text{out}}}{P_{p,\text{in}}} = \frac{T_p v_a}{2\pi M_p n_p} = \frac{K_T}{K_Q}\frac{J}{2\pi}, \tag{53}$$

and advance coefficient

$$J = \frac{v_a}{n_p D_p} = \frac{(1-f_w)v}{n_p D_p}, \tag{54}$$

where D_p is the diameter of the propeller, n_p is the shaft speed, M_p is the shaft torque, $P_{p,\text{out}}$ is the thrust power and $P_{p,\text{in}}$ is the shaft input power [22].

The advance speed v_a describes the average speed of the water across the surface of the propeller. Due to the interaction of the hull with the surrounding water, the advance speed is lower than the vessel speed. This is mathematically expressed through the wake fraction coefficient f_w and the relation between advance and vessel speed is given in equation (54).

GP compatible propeller model is derived by second-order polynomial approximation of K_T and K_Q coefficients. The second-order approximations are expressed as:

$$K_T = a_{T0} - a_{T2} J^2, \tag{55}$$

$$K_Q = a_{Q0} - a_{Q2} J^2, \tag{56}$$

where $a_{T0}, \ldots, a_{Q2}$ are coefficients of the polynomials.

The second-order approximation of K_T yields the thrust equation

$$\begin{aligned} T_p &= K_T \rho_{\text{sw}} D_p^4 n_p^2 \\ &= \left[a_{T0} - a_{T2} \left(\frac{v_a}{n_p D_p} \right)^2 \right] \rho_{\text{sw}} D_p^4 n_p^2 \\ &= \rho_{\text{sw}} D_p^2 \left(a_{T0} D_p^2 n_p^2 - a_{T2} v_a^2 \right). \end{aligned} \tag{57}$$

The total required thrust generated by the propeller exceeds the resistance R_T due to the sucking action of the rotating propeller [22]. Thrust deduction coefficient t_{TD} accounts for this effect:

$$t_{\text{TD}} = 1 - \frac{R_T}{T_p} \Rightarrow T_p = \frac{R_T}{1 - t_{\text{TD}}}. \tag{58}$$

Combining (57) and (58) gives the propeller speed as a function of towing resistance:

$$n_p^2 = \frac{R_T/(1-t_{\text{TD}}) + \rho_{\text{sw}} a_{T2} v_a^2 D_p^2}{\rho_{\text{sw}} a_{T0} D_p^4}. \tag{59}$$

The torque equation is

$$M_p = K_Q \rho_{\text{sw}} D_p^5 n_p^2 = \rho_{\text{sw}} D_p^3 \left(a_{Q0} D_p^2 n_p^2 - a_{Q2} v_a^2 \right). \tag{60}$$

By substituting n_p^2 in (59) to the torque equation and relaxing the equation to inequality constraint yields

$$M_p \geq D_p \frac{a_{Q0}}{a_{T0}} \frac{R_T}{1-t_{\text{TD}}} + \rho_{\text{sw}} v_a^2 D_p^3 \left(\frac{a_{Q0} a_{T2}}{a_{T0}} - a_{Q2} \right), \tag{61}$$

where $\left(a_{Q0} a_{T2}/a_{T0} - a_{Q2}\right) > 0$ ensures that the right-hand side is a posynomial and the inequality is GP compatible.

The model formulation above applies the propeller as a single-screw plant. The towing resistance is allocated evenly to both propellers in the case of a twin-screw plant.

G. PROPULSION MOTORS

Various electric machine types fulfil the propulsion motor requirements for vessels. Synchronous electric machines with permanent excitation usually operate more efficient than other machine types of comparable rating, since the resistive losses in order to excite the air gap magnetic field are reduced [26]. The power losses in electric machines can be divided into copper (resistive) losses, iron (magnetization) losses, bearing friction losses, windage (drag) losses

and additional losses. In Permanent Magnet Synchronous Machines (PMSMs), copper losses occur only in the stator windings and depend on the square of the stator current. Moreover, in PMSMs, iron losses mainly occur in the stator as the rotor turns synchronously with the rotating magnetic field. Iron losses are proportional to the square of the magnetic field density as well as to the square of the magnetic field frequency. Bearing friction losses can be assumed proportional to the angular speed of the shaft [26]. Windage losses are the result of drag forces on rotating surfaces and therefore proportional to the cube of the shaft speed. The additional losses include various losses that are not considered in the other categories, mainly due to eddy currents caused by the time and space harmonics of the magnetic field. The additional losses can be therefore assumed proportional to the square of the magnetic field density and the square of the magnetic field frequency like the iron losses.

Let M_N be the nominal shaft torque and n_N be the nominal (mechanical) speed of an electric machine. Therefore, (n_N, M_N) corresponds to the nominal operating point and $P_N = 2\pi M_N n_N$ to the nominal shaft power. Using the per unit (pu) system, power can be expressed as a proportion of the nominal power [27]. For instance, if the total power losses of the machine at the nominal operating point are $P_{L,N}$, the per unit total power losses are $p_{L,n} = P_{L,N}/P_N$. Let $p_{N,\mathrm{Cu}}$ be the per unit copper losses in the stator at nominal load that can be measured through a short circuit test. Moreover, let $p_{N,\mathrm{FeO}}$ be the pu iron losses at nominal speed and no-load that can be measured through a no-load test. Further, let $p_{N,\mathrm{fr}}$ be the pu friction losses and $p_{N,w}$ be the pu windage losses at nominal speed, which can be estimated through a no-load test. Furthermore, let $p_{N,\mathrm{add}}$ be the pu additional losses at the nominal operating point, which correspond to the difference between the total measured losses $p_{L,N}$ and the sum of the losses $p_{N,\mathrm{Cu}}$, $p_{N,\mathrm{Fe0}}$, $p_{N,\mathrm{fr}}$ and $p_{N,w}$ at the nominal operating point. When PMSMs are driven under field-oriented control that imposes maximum torque per stator current, the stator current is roughly proportional to the shaft torque. Therefore, according to the dependence of each power loss category on speed and load, the per unit power losses of a PMSM at the operating point (n_p, M_p) approximate

$$\begin{aligned} p_L = p_L\left(n_p,\ M_p\right) = p_{N,\mathrm{Cu}}\left(\frac{M_p}{M_N}\right)^2 \\ + p_{N,\mathrm{Fe0}}\left(\frac{n_p}{n_N}\right)^2 + p_{N,\mathrm{fr}}\left(\frac{n_p}{n_N}\right) \\ + p_{N,w}\left(\frac{n_p}{n_N}\right)^3 + p_{N,\mathrm{add}}\left(\frac{n_p}{n_N}\right)^2\left(\frac{M_p}{M_N}\right)^2, \end{aligned} \tag{62}$$

where M_p/M_N is the per unit torque and n_p/n_N is the per unit speed. A similar method to estimate the pu power losses at any operating point is described in the standard IEC 60034-2-3 [28], which, however, requires measurements at seven operating points.

H. POWER CONVERTER

Permanent magnet synchronous machines are usually driven by dedicated power converters, which facilitate operation at variable speed. Power losses in semiconductor-based power converters can be divided into conduction and switching losses. Considering that the switching frequency of semiconductors is usually constant, power converter losses are approximately proportional to the square of the semiconductor current. The nominal power converter losses $P_{L,N,\mathrm{pc}}$ correspond to the power losses at the nominal power converter current $I_{N,\mathrm{pc}}$ and therefore at the nominal power converter power $S_{N,\mathrm{pc}}$. Manufacturers usually specify the nominal power converter losses in order to facilitate the design of cooling systems. The pu power converter losses are defined as $p_{L,\mathrm{pc}} = P_{L,\mathrm{pc}}/S_{N,\mathrm{pc}}$, where $P_{L,\mathrm{pc}}$ denotes the power converter losses. Considering that the power converter current is rated as high as the rated current of the electric machine, nominal current in the power converter corresponds roughly to nominal torque on the shaft of the electric machine. Therefore, the pu power losses of power converters can be expressed as a function of the power converter current I_{pc}, which is roughly proportional to the shaft torque of the electric machine they drive, that is

$$p_{L,\mathrm{pc}} = p_{L,N,\mathrm{pc}}\left(\frac{I_{\mathrm{pc}}}{I_{N,\mathrm{pc}}}\right)^2 \approx p_{L,N,\mathrm{pc}}\left(\frac{M_p}{M_N}\right)^2. \tag{63}$$

Power converters with a rated power over 100 kVA usually have a nominal efficiency that ranges between 97% and 99%. Therefore, $p_{L,N,\mathrm{pc}}$ lies in the 0.01…0.03 pu range.

I. BATTERY ENERGY STORAGE

The battery is modeled at the level of cells, which are described by an open circuit voltage and a series resistance. A linear approximation of the open circuit voltage u with respect to discharged capacity $\bar{q}$ gives the cell model:

$$u = u_0 - k_{\mathrm{dv}}\bar{q}, \tag{64}$$

$$\dot{\bar{q}} = i, \tag{65}$$

where u_0 is the line intersection of the linear approximation (Fig. 6), k_{dv} is the negative of differential voltage $(-du/d\bar{q})$ and i is the cell current. Fig. 6 illustrates that the linear approximation is valid for the normal operating region of the cell because the strongly nonlinear parts lie outside the lower and upper bounds.

The battery pack is assembled from large number of cells arranged in series and parallel. However, the cell current for a given discharge power does not depend on the particular arrangement. Using chain rule, we can write the discharged energy E with n_{cell} total number of cells as

$$\begin{aligned} E &= n_{\mathrm{cell}}\int_0^{\bar{q}} u(\bar{q}')\,d\bar{q}' = n_{\mathrm{cell}}\left(u_0\bar{q} - \frac{1}{2}k_{\mathrm{dv}}\bar{q}^2\right) \\ &= n_{\mathrm{cell}}\frac{1}{2k_{\mathrm{dv}}}(u_0^2 - u^2) \end{aligned} \tag{66}$$

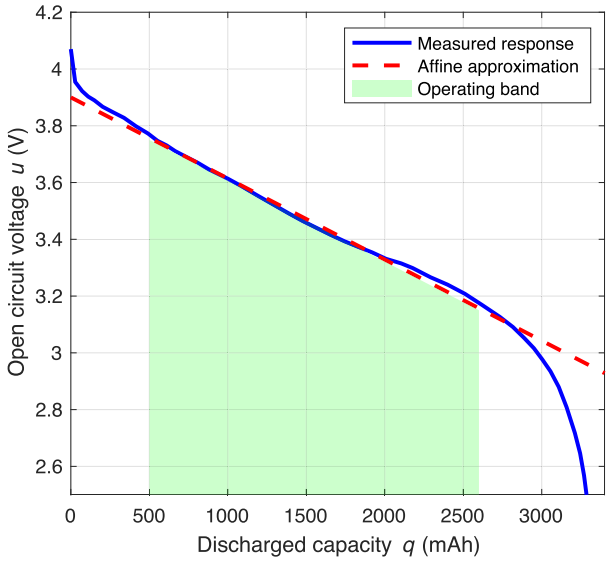

FIGURE 6. Discharge characteristics of a lithium-ion cell.

and its derivative as

$$\dot{E} = \frac{dE}{dt} = \frac{dE}{d\bar{q}}\dot{\bar{q}} = n_{\text{cell}} u i = P_{\text{bp}} + P_{L,\text{bp}}, \tag{67}$$

where P_{bp} is the battery pack terminal power and $P_{L,\text{bp}}$ is the dissipation power.

The dissipation power due to cell internal and contact resistance R_{cell} increases with the square of the current:

$$\begin{aligned} P_{L,\text{bp}} &= n_{\text{cell}} R_{\text{cell}} i^2 = R_{\text{cell}} \frac{(P_{\text{bp}} + P_{L,\text{bp}})^2}{n_{\text{cell}} u^2} \\ &= R_{\text{cell}} \frac{P_{L,\text{bp}}^2 + 2P_{L,\text{bp}}P_{\text{bp}} + P_{\text{bp}}^2}{n_{\text{cell}} u_0^2 - 2k_{\text{dv}} E}. \end{aligned} \tag{68}$$

Rearranging the terms and relaxing the constraint gives the posynomial inequality

$$\frac{n_{\text{cell}} u_0^2}{R_{\text{cell}}} \geq \frac{2Ek_{\text{dv}}}{R_{\text{cell}}} + P_{L,\text{bp}} + 2P_{\text{bp}} + \frac{P_{\text{bp}}^2}{P_{L,\text{bp}}}. \tag{69}$$

The derivative of the posynomial on the right-hand side of (69) with respect to $P_{L,\text{bp}}$ is $1 - P_{\text{bp}}^2/P_{L,\text{bp}}^2$. Thus, decrease in $P_{L,\text{bp}}$ increases the right-hand side of the inequality and drives it tight under the condition that

$$\begin{aligned} &P_{\text{bp}} > P_{L,\text{bp}} \\ &\quad \Rightarrow (u_0 - k_{\text{dv}}\bar{q}_{\max}) i_{\max} - R_{\text{cell}} i_{\max}^2 > R_{\text{cell}} i_{\max}^2 \\ &\quad \Rightarrow u_0 > 2R_{\text{cell}} i_{\max} + k_{\text{dv}} \bar{q}_{\max}. \end{aligned} \tag{70}$$

The condition is trivially satisfied by typical lithium-ion cells. The inequality (69) will hold as equality at the optimal solution of any problem that minimizes battery discharged energy (e.g., by minimizing n_{cell}).

Constraints on the discharged energy follow from the bounds of allowed cell operating region $[\bar{q}_{\min}, \bar{q}_{\max}]$:

$$n_{\text{cell}} \left(u_0 \bar{q}_{\min} - \frac{k_{\text{dv}} \bar{q}_{\min}^2}{2} \right) \leq E \tag{71}$$

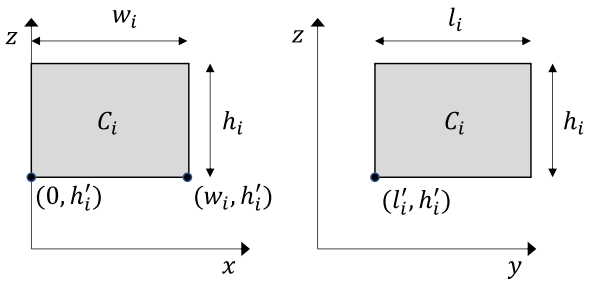

FIGURE 7. Coordinates of cuboid spaces.

$$E \leq n_{\text{cell}} \left(u_0 \bar{q}_{\max} - \frac{k_{\text{dv}} \bar{q}_{\max}^2}{2} \right). \tag{72}$$

Permissible discharging current $i_{\max}$ imposes a bound on the discharging power via the power dissipation:

$$P_{L,\text{bp}} \leq n_{\text{cell}} R_{\text{cell}} i_{\max}^2. \tag{73}$$

J. GENERAL ARRANGEMENT

The hull is subdivided to watertight compartments via transverse walls, called bulkheads. Necessary elements include collision bulkhead, fore and aft machinery room dividers and aft bulkhead [4]. We consider the number of the bulkheads as given.

Let $C_1, \ldots, C_{N_{\text{space}}}$ denote N_{space} cuboid spaces, called *blocks*, assigned to different productive functions. These include, but are not limited to, cargo holds, propulsion motors and battery energy storage. The problem concerns the placement and configuration of the dimensions of the blocks. The problem formulation exploits known convexity properties of placement problems [10] (Ch. 8).

The ith block is specified by its width w_i, length l_i, height h_i and left lower corner (w_i', l_i', h_i') in relation to the origin located at the keel centerline of the foremost part of hull (Fig. 7). The dimensions relate to the volume via monomial equations:

$$w_i l_i h_i = V_i \tag{74}$$

for each $i = 1, \ldots, N_{\text{space}}$. Here, V_i depends on the installed power rating or capacity of the equipment corresponding to the function the block belongs to. A block i can be similar to another block j, $i \neq j$, by a variable scaling ratio $s_{i,j}$:

$$x_i = s_{i,j} x_j, \quad x \in \{w, l, h\}. \tag{75}$$

A block is placed inside a bounding box with width B, length L and height D, which are the hull principal dimensions. The bounding box constraints are:

$$w_i' + w_i \leq B/2, \quad h_i' + h_i \leq D, \quad l_i' + l_i \leq L \tag{76}$$

for each $i = 1, \ldots, N_{\text{space}}$. The placement of the blocks is also constrained by the geometry of the relevant hull sections.

The blocks do not overlap except at the boundaries. At least one of the following relations holds for each $i \neq j$:

$$C_i \text{ is left or right of } C_j,$$
$$C_i \text{ is above or below of } C_j,$$
$$C_i \text{ is front or behind of } C_j.$$

The relative positioning constraints are written as:

$$w_i' + w_i \leq w_j', \quad \forall (i,j) \in \Lambda_X \tag{77}$$

where Λ_X is the set of adjacent blocks meaning that C_i is to the left of C_j if $(i,j) \in \Lambda_X$. Similar positioning constraints hold for pairs above/below and front/behind. Bounding box, overlap and relative positioning constraints are posynomial inequalities.

Tanks for ballast water occupy spaces between the outer hull and the bottom decks of the battery spaces and the cargo hold. In the double hull design, the spaces between the cargo hold walls and the hull can also carry ballast water. The ballast tanks are not configured explicitly in the presented optimization framework, but a constraint can be imposed on the distance from keel to the bottom deck to ensure adequate space for the tanks.

V. NUMERICAL DESIGN EXAMPLE

A. CASE DESCRIPTION

1) VESSEL CONFIGURATION

In this section, we formulate and solve a design problem within the GP framework. We consider the design of battery-electric short-sea vessel for the transport of dry bulk at low speed. The hull is assembled from the fore, midship and aft sections as presented in Sec. IV-B. The propulsion system is a twin-shaft direct drive configuration with a single propulsion motor driving each propeller. The total mass breaks down into a sum of hull, bulkhead, deck, deckhouse, cargo hold, driveline, and battery masses. Component masses are linear functions of nominal sizes.

In the all-electric vessel of the present design study, electrical energy stored in batteries is the main source of energy for propulsion motors and auxiliary loads. In this case two independent systems, located in separate spaces, are required according to classification society redundancy rules [14]. The battery packs are located in spaces at the midship and aft sections. Both systems must have sufficient capacity for a typical operation cycle.

2) REQUIREMENTS

The specified endurance, i.e., range between charging opportunity is 456 nmi (848 km) at 13 kn. The required dry bulk ($\rho_{\text{cargo}} = 0.77$ t/m^3) cargo carrying capacity is $W_{\text{cargo}} \geq 4600$ t. Independent of specific operation profile, the vessel is required to attain speed 16 kn.

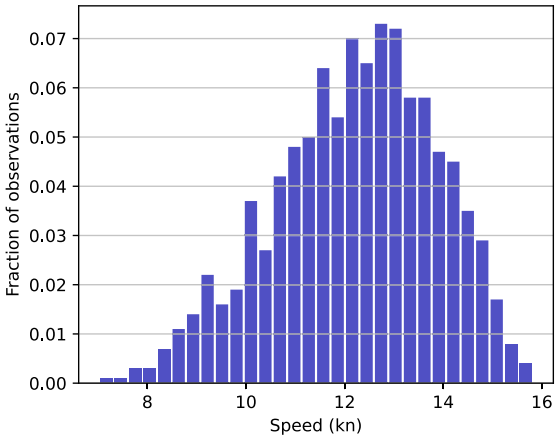

FIGURE 8. Leg speed distribution.

3) OBJECTIVE

We consider a single merit criterion for the design. The objective is to minimize the size of the battery pack, which translates to minimizing total number of cells: $f_{\text{obj}} = n_{\text{cell}}$.

4) OPERATION PROFILE

The voyage is split to 20 legs with varying speed along each leg. The speeds are sampled from distribution $6 + 10 \cdot \text{Beta}(5, 3)$, which agrees with observed speeds of a general cargo vessel reported in [29]. Fig. 8 shows a histogram of 1000 values sampled from the distribution. The leftmost panel in Fig. 11 shows the vessel speed over time.

The decision variables relating to operation are defined as vectors with 20 elements. The constraints involving these variables are enforced for each leg with index $t = 1, \ldots, 20$. However, the indexing is omitted in the problem formulation (Sec. V-B) for sake of clarity. The only exception is the discrete-time battery energy update, which relates the values of E at consecutive periods

$$E(t+1) \geq E(t) + \Delta t(t)(P_{\text{bp}}(t) + P_{L,\text{bp}}(t)), \quad t = 1, \ldots, 20$$

where E is a 21-vector and Δt is a 20-vector of voyage leg sailing durations.

B. GP PROBLEM FORMULATION

The battery-electric vessel design problem is formulated as the following GP:

$$\text{min.} \quad f_{\text{obj}} = n_{\text{cell}}$$

s.t.

$$\left.\begin{aligned} &\frac{L_j}{L} = y_j,\ j \in \{\text{fore, mid, aft}\} \\ &B_{\text{WL}} = 2\left(\frac{T}{a}\right)^{1/b} \\ &2\left(\frac{D}{a}\right)^{1/b} \leq 16.5 \\ &T \leq 8.7 \\ &T + F \leq D \end{aligned}\right\} \text{Principal dimensions}$$

Displacement

$$V_{\text{mid,under}} = \frac{L_{\text{mid}} T \left(\frac{T}{a}\right)^{1/b}}{b+1}$$

$$V_{\text{fore,under}} = \frac{2L_{\text{fore}} T \left(\frac{1}{T}\right)^{-1/b}}{3(b+1)}$$

$$V_{\text{fore,res}} = \frac{L_{\text{fore}} T}{3}\left(\frac{1}{T}\right)^{-1/b}$$

$$V_{\text{aft,below}} = \frac{1}{3} V_{\text{mid,below}}$$

$$V_{\text{block}} = LTB_{\text{WL}}$$

$$\nabla \leq V_{\text{block}} - 2V_{\text{fore,below}} - 2V_{\text{fore,res}} - 2V_{\text{mid,below}} - 2V_{\text{aft,below}}$$

Wetted area

$$A_s \geq 2(L_{\text{mid}} + \frac{1}{3}(L_{\text{aft}} + L_{\text{fore}}))r_{T,\text{mid}}$$

$$r_{T,\text{mid}} \geq \sum_{i=0}^{N_{\text{arc}}-1} \sqrt{dx_{T,\text{mid}}^2 + dy_{T,\text{mid}}^2}$$

$$dx_{T,\text{mid}} = \frac{1}{N_{\text{arc}}}\left(\frac{T}{a}\right)^{1/b}$$

$$dy_{T,\text{mid}} = Tb\left(\frac{1}{2}+i\right)^{b-1}\frac{1}{N_{\text{arc}}^b}$$

Resistance

$$C_F^{3.1673} \geq 108.284(vL)^{-0.697} + 28.968(vL)^{-0.317}$$

$$R_T \geq \frac{1}{2}\rho_{\text{sw}}(C_F + C_R)A_s v^2$$

Longitudinal strength

$$I_{\text{mid}} + DBt_p^2(2\phi + n_L\eta\lambda\gamma^2) \leq \frac{t_p BD^2}{2}(2\phi + n_L\eta\gamma\lambda^2 + n_L\gamma(\tau - 2\tau^2))$$

$$M_{\text{wv+sw}} = 0.3365\, C_w BL^2$$

$$\sigma_{\text{perm}} \geq \frac{DM_{\text{wv+sw}}}{2I_{\text{mid}}}$$

Weight relations

$$W_{\text{hull}} \geq 2\rho_{\text{steel}} t_p (L_{\text{mid}} + \frac{1}{3}(L_{\text{aft}} + L_{\text{fore}}))r_{D,\text{mid}}$$

$$r_{D,\text{mid}} \geq \sum_{i=0}^{N_{\text{arc}}-1} \sqrt{dx_{D,\text{mid}}^2 + dy_{D,\text{mid}}^2}$$

$$dx_{D,\text{mid}} = \frac{1}{N_{\text{arc}}}\left(\frac{D}{a}\right)^{1/b}$$

$$dy_{D,\text{mid}} = Db\frac{1}{N_{\text{arc}}^b}\left(\frac{1}{2}+i\right)^{b-1}$$

$$W_{\text{cargo}} \geq 4600$$

$$W_{\text{bh}} \geq 2n_{\text{bh}} t_p \rho_{\text{steel}} \frac{bD}{b+1}\left(\frac{D}{a}\right)^{(1/b)}$$

$$W_{\text{deck}} \geq t_p \rho_{\text{steel}}\left[L_{\text{mid}}B + L_{\text{fore}}\frac{2}{3}\left(\frac{D}{a}\right)^{1/b}\right]$$

$$W_{\text{wall}} = t_p\rho_{\text{steel}}(2l_{\text{cargo}}h_{\text{cargo}} + 4w_{\text{cargo}}h_{\text{cargo}} + 2w_{\text{cargo}}l_{\text{cargo}})$$

$$W_{\text{power}} \geq 4\pi n_N M_N W_{\text{em+pc}}$$

$$W_{\text{bp}} = n_{\text{cell}} W_{\text{cell}}$$

$$\nabla\rho_{\text{sw}} \geq W_{\text{hull}} + 2W_{\text{bp}} + W_{\text{cargo}} + W_{\text{drive}} + W_{\text{deck}} + W_{\text{wall}} + W_{\text{bh}} + W_{\text{dh}}$$

Cargo hold

$$h'_{\text{cargo}} = L_{\text{fore}}^{b/2} a \frac{w_{\text{cargo}}^b}{l'^{b/2}}$$

$$\frac{W_{\text{cargo}}}{\rho_{\text{cargo}}} = 2w_{\text{cargo}}l_{\text{cargo}}h_{\text{cargo}}$$

$$l'_{\text{cargo}} + l_{\text{cargo}} \leq (y_{\text{fore}} + y_{\text{mid}})L$$

$$h'_{\text{cargo}} + h_{\text{cargo}} \leq D$$

Midship battery space

$$h'_{\text{bp}} = L_{\text{fore}}^{b/2} a \frac{w_{\text{bp}}^b}{l'^{b/2}_{\text{bp}}}$$

$$n_{\text{cell}} V_{\text{bp}} = 2w_{\text{bp}}l_{\text{bp}}h_{\text{bp}}$$

$$l'_{\text{bp}} + l_{\text{bp}} \leq (y_{\text{fore}} + y_{\text{mid}})L$$

$$h'_{\text{bp}} + h_{\text{bp}} \leq h'_{\text{cargo}}$$

$$h'_{\text{bp}} \geq h'_{\text{bp,min}},\ h_{\text{bp}} \geq h_{\text{bp,min}}$$

Aft battery space

$$h'_{\text{bp2}} = w_{\text{bp2}}^{0.5b} a \left(\frac{D}{a}\right)^{0.5}$$

$$n_{\text{cell}} V_{\text{bp}} = 2w_{\text{bp2}}l_{\text{bp2}}h_{\text{bp2}}$$

$$h'_{\text{bp2}} + h_{\text{bp2}} \leq D$$

$$h'_{\text{bp2}} \geq h'_{\text{bp,min}}$$

Stability

$$\frac{(b+1)(T/a)^{2/b}}{3Tb} \geq (z_{\text{safe}} - 1)\frac{T(b+1)}{2b+1} + z_{\text{GK}}$$

$$z_{\text{GK}} \geq (l'_{\text{cargo}} + \frac{1}{2}l_{\text{cargo}})$$

Propulsion

$$v_a = (1 - f_w)v$$

$$\frac{1}{2}D_p \leq T$$

$$M_p \geq D_p \frac{a_{Q0}}{a_{T0}}\frac{R_T}{1 - t_{\text{TD}}} + \rho_{\text{sw}} v_a^2 D_p^3\left(\frac{a_{Q0}a_{T2}}{a_{T0}} - a_{Q2}\right)$$

$$n_p^2 \geq \frac{R_T/(1 - t_{\text{TD}}) + \rho_{\text{sw}} a_{T2} v_a^2 D_p^2}{\rho_{\text{sw}} a_{T0} D_p^4}$$

Energy storage

$$P_{\text{bp}} \geq 4\pi\left[(p_{L,\text{em}} + p_{L,\text{pc}})n_N M_N + n_p M_p\right] + P_A$$

$$E(t+1) \geq E(t) + \Delta t(t)(P_{\text{bp}}(t) + P_{L,\text{bp}}(t))$$

$$\frac{n_{\text{cell}}u_0^2}{R_{\text{cell}}} \geq \frac{2Ek_{\text{dv}}}{R_{\text{cell}}} + P_{L,\text{bp}} + 2P_{\text{bp}} + \frac{P_{\text{bp}}^2}{P_{L,\text{bp}}}$$

$$E(21) \leq n_{\text{cell}}\left(u_0\bar{q}_{\max} - \frac{k_{\text{dv}}\bar{q}_{\max}^2}{2}\right)$$

$$E(1) \geq n_{\text{cell}}\left(u_0\bar{q}_{\min} - \frac{k_{\text{dv}}\bar{q}_{\min}^2}{2}\right)$$

Powertrain

$$p_{L,\text{em}} \geq p_{N,\text{Cu}}\left(\frac{M_p}{M_N}\right)^2 + p_{N,\text{Fe0}}\left(\frac{n_p}{n_N}\right)^2 + p_{N,\text{fr}}\left(\frac{n_p}{n_N}\right) + p_{N,w}\left(\frac{n_p}{n_N}\right)^3 + p_{N,\text{add}}\left(\frac{n_p}{n_N}\right)^2\left(\frac{M_p}{M_N}\right)^2$$

$$p_{L,\text{pc}} \geq p_{L,N,\text{pc}}\left(\frac{M_p}{M_N}\right)^2$$

$$M_p \leq 1.6M_N,\ n_p \leq 1.6n_N,\ M_p n_p \leq M_N n_N.$$

TABLE 1. Subscript nomenclature in the problem formulation.

Subscript	Description
bp	battery pack
deck	weather (uppermost) deck
wall	cargo hold walls and bottom
power	powertrain
bh	bulkhead
dh	deckhouse

TABLE 2. Breakdown of power loses by category for a three-phase 12-pole water-cooled PMSM rated at 160 kW, 1500 r/min and 1019 Nm [30].

Loss group	Symbol	Power losses relative to nominal power (%)
Copper	$p_{N,\mathrm{Cu}}$	2.19
Iron	$p_{N,\mathrm{Fe0}}$	0.77
Windage	$p_{N,w}$	0.45
Friction	$p_{N,\mathrm{fr}}$	0.12
Residual	$p_{N,\mathrm{add}}$	0.25

Table 1 defines the new subscripts in the problem formulation above.

C. ELECTRIC MACHINE LOSS FUNCTION PARAMETRIZATION

The power losses of a three-phase 12-pole PMSM with buried rotor magnets rated at 160 kW, 1500 r/min and 1019 Nm are used to parametrize the loss function (62) [30]. The stator of the 12-pole PMSM is water-cooled, however, the consumption of the cooling system is not considered in the machine losses. Table 2 breaks down the power losses of the 12-pole PMSM by category at the nominal operating point. Since friction and windage losses were not identified separately in [30], a share of 20% for friction losses and a share of 80% for windage losses is assumed.

According to the loss breakdown presented in Table 2, the nominal efficiency of the electric machine for motor operation, which is defined as the ratio of shaft power to electric power at the nominal operating point, is 96.36%. The size of the electric machine is not fixed but an optimization variable. However, considering that the rated power of the electric machine remains in the range of a few hundred kW, the loss breakdown presented in Table 2 can be assumed unchanged.

For the loss function defined in (62) and the power loss shares listed in Table 2, the efficiency map of the PMSM over pu torque and pu speed is shown in Fig. 9. Torque over 1 pu corresponds to overload and speed over 1 pu corresponds to operation in field weakening. The nominal operating point (n_N, M_N) corresponds to the nominal efficiency of 96.36%, however, the motor operates with an efficiency over 96.5% at nominal speed and a torque between 0.7 pu and 0.8 pu. For operating points with a torque greater than 0.25 pu and a speed greater than 0.3 pu, the machine operates with an efficiency of over 90%. As expected, low shaft power corresponds to low efficiency.

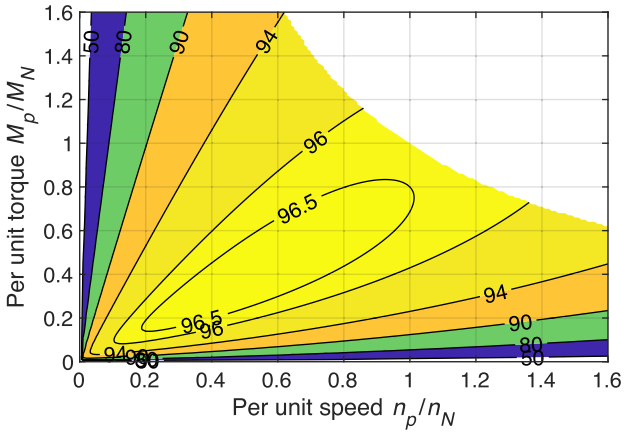

FIGURE 9. Estimated efficiency map of a three-phase 12-pole water-cooled PMSM rated at 160 kW, 1500 r/min and 1019 Nm over per unit torque and per unit speed [30]. The efficiency is given as a percentage of the ratio of shaft power to electric power. Torque over 1 per unit corresponds to overload and speed over 1 per unit corresponds to operation in field weakening.

D. SOLUTION OF THE DESIGN OPTIMIZATION PROBLEM

The GP vessel design problem is formulated with CVXPY [16] modeling language and solved with the primal-dual interior point algorithm implemented in the solver ECOS [17]. Table 3 shows values of selected fixed parameters for the problem instance. The solver computed the global optimum in less than 0.17 s on a standard desktop computer for the problem instance with 208 decision variables and 209 constraints.

The optimal values of scalar design variables are listed in Table 5. Fig. 10 illustrates the hull geometry of the optimal design and the dimensions of the battery (green), cargo (red) and propulsion motor (blue) spaces. Fig. 11 shows the optimal values of the vector variable E^* divided by the number of cells (center) and cell voltage as a function of current (right).

E. SENSITIVITIES

When a convex optimization problem is solved using primal-dual interior point solver, the optimal dual variable values are obtained for free. The local sensitivity of the objective function to each fixed parameter can be obtained from the dual solution, as discussed in Sec. III-D and [20]. The sensitivities are useful for guiding the naval architect to focus on the most important design decisions. Table 4 shows the sensitivities to selected input parameters for the vessel design problem instance formulated above.

A sensitivity of $+1$ means that increasing the parameter value by 1% increases the objective function value (number of cells) by 1%. A sensitivity of zero indicates that those constraints that include the parameter are inactive at the optimum and do not govern the solution. The minimum freeboard, stability safety margin and maximum cell discharging current show zero sensitivities.

Interestingly, the cell volume sensitivity is also zero. Fig. 10 shows that the battery pack in the deck below the cargo

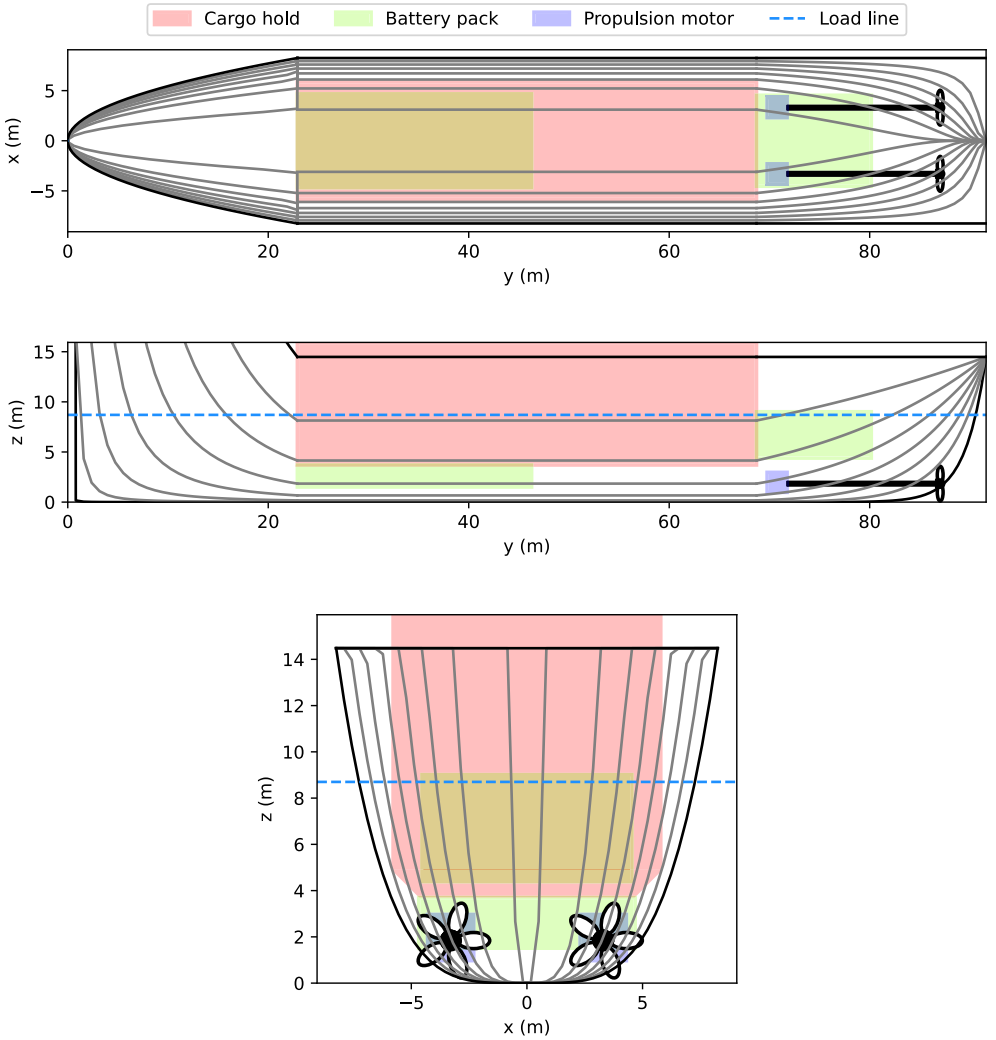

FIGURE 10. Optimal hull geometry and space allocation. Bulkheads and deckhouse in the aft section are not shown.

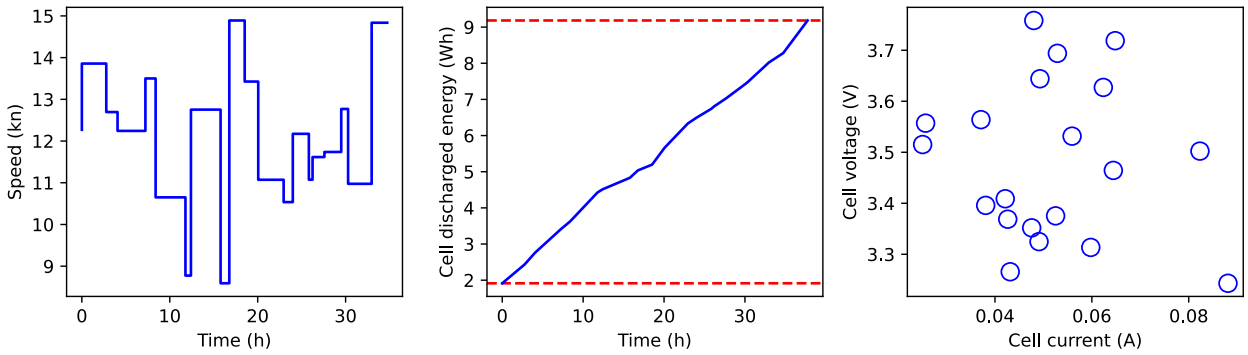

FIGURE 11. Operation profile (left), cell discharged energy (center), and cell voltage (right).

hold does not extend to the full length of the midship section. This occurs because the height of the deck below the cargo hold is constrained to a minimum 2.2 m. The pack can reserve a larger volume in the deck without any need for changes to the hull dimensions.

The sensitivity of the cell discharge upper bound exceeds one. This occurs because the higher cell capacity reduces the number of cells, and their total weight, in the optimal solution. The weight saving reduces displacement and resistance, which further reduces the required number of cells.

TABLE 3. Selected fixed constant scalar parameters for the design problem.

Quantity	Value	Description
Load carrying structures		
ϕ	0.35	bottom shell half width to hull breadth ratio
η	0.05	flange width to breadth ratio
τ	0.04	web height to hull depth ratio
γ	0.5	stiffener to bottom deck thickness ratio
n_{L}	10	number of stiffeners
σ_{perm}, N/mm^2	175	allowable deck stress
C_w	7.7	wave parameter for minimum midship section modulus
ρ_{steel}, t/m^3	8.05	steel density
Hull		
b	3.5	fullness factor
y_j	$(\frac{1}{4}, \frac{1}{2}, \frac{1}{4})$	section to overall length ratio, $j \in \{\mathrm{fore}, \mathrm{mid}, \mathrm{aft}\}$
n_{bh}	5	number of bulkheads
W_{dh}, t	1200	deckhouse mass
Stability		
z_{safe}	1.1	safety margin
F, m	1.6	minimum freeboard
Propeller		
(a_{T0}, a_{T2})	(0.3,0.35)	coefficients of K_T polynomial
(a_{Q0}, a_{Q2})	(0.041,0.041)	coefficients of K_Q polynomial
f_w	0.2	wake fraction coefficient
t_{TD}	0.15	thrust deduction coefficient
ρ_{sw}, t/m^3	1.02	seawater density
Li-ion cell		
R_{cell}, mΩ	53	internal and contact resistance
k_{dv}, V/Ah	0.286,	differential voltage
u_0, V	3.9	open circuit voltage ($\bar{q} = 0$)
$\bar{q}_{\mathrm{min}}$, Ah	0.5	minimum discharge
$\bar{q}_{\mathrm{max}}$, Ah	2.6	maximum discharge
i_{max}, A	6	allowable discharge current
Battery pack		
W_{bp}, t	0.0875	mass per 1000 cells
V_{bp}, m^3	0.118	volume per 1000 cells
Layout		
$h'_{\mathrm{bp,min}}$,m	1	minimum battery space floor separation from keel
$h_{\mathrm{bp,min}}$,m	2.2	minimum battery space wall height
Powertrain		
$W_{\mathrm{em+pc}}$, t	2.36	motor and power converter mass per MW nominal power
Hotel		
P_A, kW	150	auxiliary power

TABLE 4. Local sensitivities of selected parameters.

Quantity	Sensitivity	Quantity	Sensitivity
F	0	i_{max}	0
z_{safe}	0	ρ_{cargo}	-0.219
$\bar{q}_{\mathrm{max}}$	-1.12	b	-0.0601
V_{bp}	0	W_{bp}	0.0405
t_{TD}	0.144	f_w	0.204

The negative sensitivity of the hull fullness parameter b indicates that the design is improved by increasing the fullness, which corresponds to larger block coefficient. This agrees with typical high block coefficient values found in conventional slow bulk carriers [22]. By increasing the block coefficient, the wetted surface area is reduced relative to cargo capacity.

TABLE 5. Values of selected decision variables and derived quantities for the solved design problem.

Quantity	Value	Description
Dimensions		
L, m	91.6	length overall
D, m	14.5	depth
B, m	16.5	breadth
T, m	8.7	scantling draught
Hull		
a	3.13×10^{-3}	lateral scaling factor
t_p, mm	10.7	deck plate thickness
∇, m^3	6175	displacement volume
A_s, m^2	1767	wetted surface area
Propeller		
D_p, m	3.48	diameter
Energy storage		
n_{cell}	4086	lithium-ion cells (thousands)
ΔE, MWh	29.7	discharged energy
$2W_{\mathrm{bp}}/W_{\mathrm{cargo}}$	0.155	battery to cargo mass ratio
Powertrain		
M_N, kNm	103	nominal motor torque
$60n_N$, r/min	189	nominal motor speed
P_N, kW	2039	nominal motor power

VI. CONCLUSION

This paper presented a novel approach to conceptual-stage design optimization of battery-electric marine vessels. By using posynomial forms for all subsystem models, the optimization problem can then be formulated as a geometric program, enabling the use of convex optimization tools to efficiently search the design space.

While the method has been demonstrated using only continuous decision variables, in practical vessel design many decisions are distinct or involve discrete quantities. Typical discrete decisions are the positions of spaces with respect to each other in the general arrangement, the number of car lanes in RoPax ferries, installed sizes of components and component on/off switching over time. Incorporating discrete decisions to the presented framework should be explored in future work.

The discrete decisions are modeled mathematically by integer variables that give rise to a nonconvex feasible set. A problem that follows the GP form with respect to log-convex functions but which features both continuous and discrete variables belongs to the class of optimization problems called convex mixed-integer nonlinear programs (MINLP). A convex MINLP exhibits desirable properties that can be exploited by solution methods, namely, relaxing the integrality requirements yields a convex problem. Thus, it is possible to solve a convex MINLP exactly by decomposing it into a finite sequence of convex subproblems, which is not necessarily true for a general MINLP problem [31]. Nevertheless, the solution times for convex MINLPs are many orders of magnitude greater compared to convex problems.

While methods for solving convex problems are considered mature technology, methods for convex MINLPs are still undergoing active development and rapid improvement. Standard methods for solving convex MINLPs are described, for example, in [31]. Solvers employing these methods include SHOT [32], AOA [33] and BARON [34]. A recent survey revealed significant performance differences between the solvers [35].

REFERENCES

[1] F. Ueckerdt, C. Bauer, A. Dirnaichner, J. Everall, R. Sacchi, and G. Luderer, "Potential and risks of hydrogen-based e-fuels in climate change mitigation," *Nature Climate Change*, vol. 11, no. 5, pp. 384–393, May 2021.
[2] J. Kersey, N. D. Popovich, and A. A. Phadke, "Rapid battery cost declines accelerate the prospects of all-electric interregional container shipping," *Nature Energy*, vol. 7, no. 7, pp. 664–674, Jul. 2022.
[3] *Batteries on Board Ocean-Going Vessels*, MAN, Munich, Germany, 2020.
[4] S. Hirdaris, *Lecture Notes on Basic Naval Architecture*. Espoo, Finland: Aalto Univ., 2021.
[5] A. Papanikolaou, *Ship Design Methodologies of Preliminary Design*. Cham, Switzerland: Springer, 2014.
[6] C. A. Frangopoulos, "Developments, trends, and challenges in optimization of ship energy systems," *Appl. Sci.*, vol. 10, no. 13, p. 4639, Jul. 2020.
[7] G. Sakalis, G. Tzortzis, and C. Frangopoulos, "Intertemporal static and dynamic optimization of synthesis, design, and operation of integrated energy systems of ships," *Energies*, vol. 12, no. 5, p. 893, Mar. 2019.
[8] H. Nowacki, "Five decades of computer-aided ship design," *Comput.-Aided Des.*, vol. 42, no. 11, pp. 956–969, Nov. 2010.
[9] B. Molchanov, T. Lien, and M. Elg, *New Design Methods for Low-Carbon Shipping*. Espoo, Finland: VTT Technical Research Centre of Finland, 2021.
[10] S. Boyd, S. P. Boyd, and L. Vandenberghe, *Convex Optimization*. Cambridge, U.K.: Cambridge Univ. Press, 2004.
[11] V. F. Pavlidis, E. G. Friedman, and I. Savidis, *Three-Dimensional Integrated Circuit Design*. Amsterdam, The Netherlands: Elsevier, 2017.
[12] R. A. Jabr, "Application of geometric programming to transformer design," *IEEE Trans. Magn.*, vol. 41, no. 11, pp. 4261–4269, Nov. 2005.
[13] W. Hoburg and P. Abbeel, "Geometric programming for aircraft design optimization," *AIAA J.*, vol. 52, no. 11, pp. 2414–2426, Nov. 2014.
[14] *Rules for Classification, Ships—Part 6 Additional Class Notation. Chapter 2 Propulsion, Power Generation and Auxiliary Systems*, DNV, Bærum, Norway, 2020.
[15] M. Grant and S. Boyd. (2014). *CVX: MATLAB Software for Disciplined Convex Programming, Version 2.1*. [Online]. Available: http://cvxr.com/cvx/
[16] S. Diamond and S. Boyd, "CVXPY: A Python-embedded modeling language for convex optimization," *J. Mach. Learn. Res.*, vol. 17, no. 83, pp. 1–5, Apr. 2016.
[17] A. Domahidi, E. Chu, and S. Boyd, "ECOS: An SOCP solver for embedded systems," in *Proc. Eur. Control Conf. (ECC)*, Jul. 2013, pp. 3071–3076.
[18] B. Stellato, G. Banjac, P. Goulart, A. Bemporad, and S. Boyd, "OSQP: An operator splitting solver for quadratic programs," *Math. Program. Comput.*, vol. 12, no. 4, pp. 637–672, Dec. 2020.
[19] B. O'Donoghue, E. Chu, N. Parikh, and S. Boyd, "Conic optimization via operator splitting and homogeneous self-dual embedding," *J. Optim. Theory Appl.*, vol. 169, no. 3, pp. 1042–1068, Jun. 2016.
[20] R. S. Dembo, "Sensitivity analysis in geometric programming," *J. Optim. Theory Appl.*, vol. 37, no. 1, pp. 1–21, May 1982.
[21] W. Hoburg, P. Kirschen, and P. Abbeel, "Data fitting with geometric-programming-compatible softmax functions," *Optim. Eng.*, vol. 17, no. 4, pp. 897–918, Dec. 2016.
[22] "Basic principles of ship propulsion," MAN Energy Solutions, Copenhagen, Denmark, Tech. Rep., 2018.
[23] "ITTC—Recommended procedures and guidelines—Resistance test," DNV, Int. Towing Tank Conf., Zürich, Switzerland, Tech. Rep. 7.5-02-02-01, 2011.
[24] P. Varsta, H. Remes, and J. Romanoff, *Global Hull-Girder Response (Quasi-Static, Prismatic Beam Models)*. Hoboken, NJ, USA: Wiley, 2017.
[25] "Rules for classification: Ships—DNV-RU-ship pt.3 CH.5.," DNV, Bærum, Norway, Tech. Rep., 2021.
[26] T. Jokinen, V. Hrabovcova, and J. Pyrhonen, *Design of Rotating Electrical Machines*. Hoboken, NJ, USA: Wiley, 2013.
[27] P. S. Kundur and O. P. Malik, *Power System Stability and Control*. New York, NY, USA: McGraw-Hill, 2022.
[28] *Rotating Electrical Machines—Part 2-3: Specific Test Methods for Determining Losses and Efficiency of Converter-Fed AC Motors*, Standard ISO/IEC 60034-2-3:2020, International Organization for Standardization, Geneva, Switzerland, 2020.
[29] F. Baldi, "Modelling, analysis and optimisation of ship energy systems," Ph.D. thesis, Dept. Shipping Mar. Technol., Chalmers Univ. Technol., Gothenburg, Sweden, 2016.
[30] B. Deusinger, "Indirect efficiency determination and parameter identification of permanent magnet synchronous machines," Ph.D. thesis, Dept. Elect. Eng. Inf. Technol., Tech. Univ. Darmstadt, Darmstadt, Germany, 2021.
[31] J. Kronqvist, "Polyhedral outer in approximations convex mixed-integer nonlinear programming," Ph.D. thesis, Dept. Process Syst. Eng., Åbo Akademi Univ., Turku, Finland, 2018.
[32] A. Lundell, J. Kronqvist, and T. Westerlund, "The supporting hyperplane optimization toolkit for convex MINLP," *J. Global Optim.*, vol. 84, no. 1, pp. 1–41, Sep. 2022.
[33] M. Hunting, "The AIMMS outer approximation algorithm for MINLP," AIMMS, New Delhi, India, White Paper, 2011.
[34] M. Tawarmalani and N. V. Sahinidis, "A polyhedral branch-and-cut approach to global optimization," *Math. Program.*, vol. 103, no. 2, pp. 225–249, Jun. 2005.
[35] J. Kronqvist, D. E. Bernal, A. Lundell, and I. E. Grossmann, "A review and comparison of solvers for convex MINLP," *Optim. Eng.*, vol. 20, no. 2, pp. 397–455, Dec. 2018.

ANTTI RITARI received the B.Sc. and M.Sc. degrees in mechanical engineering from Aalto University, Espoo, Finland, in 2015 and 2017, respectively. His master's thesis investigated the energy efficiency of battery-electric city buses. He has been a Researcher with the Mechatronic Machine Systems Group, Aalto University, since 2018. His research is primarily focused on computationally efficient optimization-based control and design synthesis of electric powertrains in marine vessels and heavy-duty vehicles.

PANAGIOTIS MOURATIDIS received the Diploma degree in electrical and computer engineering from the Aristotle University of Thessaloniki, in 2009, and the M.Sc. degree in electrical power engineering and the D.Sc. degree in engineering from the Technical University of Darmstadt, in 2014 and 2022, respectively. His Ph.D. thesis investigated potential applications and the economic performance of hybrid energy storage systems consisting of kinetic and electrochemical storages. His current research focuses on modeling, energy management, and the economic efficiency of energy storage systems.

KARI TAMMI (Member, IEEE) received the M.Sc., Lic.Sc., and D.Sc. degrees from the Helsinki University of Technology, in 1999, 2003, and 2007, respectively. He received a Teacher's pedagogical qualification at the Hame University of Applied Sciences, in 2017. He was a Researcher with CERN, the European Organization for Nuclear Research, from 1997 to 2000, and a Postdoctoral Researcher with North Carolina State University, USA, from 2007 to 2008. From 2000 to 2015, he was a Research Professor, a Research Manager, the Team Leader, and other positions at the VTT Technical Research Centre of Finland. He has been an Associate Professor with Aalto University, since 2015. He is currently with the Finnish Administrative Supreme Court as a Chief Engineer Counselor. He has authored over 60 peer-reviewed publications cited in over 1500 other publications. He is a member of the Finnish Academy of Technology. He serves as the Deputy Chair for IFTOMM Finland.